Biointerface Research in Applied Chemistry
Open-Access Journal (ISSN: 2069-5837)

Article
Volume 14, Issue 2, 2024, 37
https://doi.org/10.33263/BRIAC142.037

Experimental and Finite Element Study of the Mechanical Behavior of Hydroxyapatite/Tricalcium Phosphate/Alumina Biocomposite

Mohammed Es-saddik [1,2], Said Laasri [3,*], Meryem Bensemlali [4], Nora Hariti [3], Abdelaziz Laghzizil [5], Mohamed Taha [2]

[1] Optics, Materials and Systems Team, Faculty of Sciences, Abdelmalek Essaâdi University, Tetouan 93000, Morocco
[2] Laboratory of thermodynamic and energetics, Faculty of Science, Ibn Zohr University, P O 8106, 80000 Hay Dakhla, Agadir, Morocco
[3] Chouaib Doukkali University, Laboratory of Engineering Sciences for Energy; ENSA-El Jadida, El Jadida 1104, Morocco
[4] Laboratory of Organic Bioorganic Chemistry and Environment, Faculty of Sciences, University Chouaib Doukkali, Morocco
[5] Laboratory of Applied Chemistry of Materials; Faculty of Sciences, Mohammed V University in Rabat, BP.1014, Rabat Morocco
* Correspondence: laasrisaid@yahoo.fr (S.L.);

Scopus Author ID 36903647500
Received: 22.01.2023; Accepted: 12.04.2023; Published: 4.02.2024

Abstract: This paper develops a hydroxyapatite/tricalcium phosphate/alumina composite sintered at different temperatures. The structure, microstructure, and mechanical properties were characterized by different techniques as a function of the calcination temperature. The sintered bioceramics were characterized by X-ray diffraction and scanning electron microscopy to identify the crystalline phases and topography involving the porosity, crystal defects, and interfaces. The 60wt%HAP/30wt%β-TCP/10wt%Al_2O_3 bioceramic has a microstructure, highly compacted, with better diametral resistance (23 MPa) was obtained at 1250°C. The Young's and shear modulus and diametral strength of this bioceramic were examined. These physical properties are also closely related to the sintering temperature of the ceramic. The distribution of the main stress fields in this composite was modeled by the finite element method, which correlated well with the experimental data. A correlation between the microstructure and the mechanical behavior as well as the relative density as a function of the sintering temperature of the bioceramics, has been established.

Keywords: Hydroxyapatite; Alumina ; Tricalcium phosphate; Sintering; Diametral strength; Bioceramic

1. Introduction

Materials based on calcium phosphates have established themselves in the field of biomaterials for orthopedic applications and have shown interesting properties of bioactivity and osteoconduction. Among them, bioceramics derived from hydroxyapatite $Ca_{10}(PO_4)_6(OH)_2$ and tricalcium phosphate (β-$Ca_3(PO_4)_2$) have been widely used as bone substitutes thanks to their perfect resorbability, and their perfect biocompatibility [1-6]. These two types of phosphate have the particularity of good osteoconduction to bone tissue. In addition, these calcium phosphates do not have the same resorption in contact with biological fluids, which is why research has adapted in recent years to the development of biomaterials consisting of a mixture of tricalcium phosphate and hydroxyapatite associated with other inert and

biocompatible materials [7-9]. Phosphocalcic bioceramics are today the most synthetic biomaterials adequate and are most commonly used during intraosseous implantation. They are generally porous to facilitate bone recolonization. In addition, morphological parameters such as porosity, pore size distribution, and shape, as well as mechanical properties of produced bioceramics, play a main key in improving the efficiency of biomaterials in tissue engineering [10-12]. Several approaches have been proposed, the most used of which consists in preparing scaffolds by adding organic additives porogens such as polyvinyl butyral (PVB) [13], and polymethyl methacrylate (PMMA) [14], which requires a well-defined cycle heating that can negatively affect the mechanical behavior of elaborated biomaterials, which is a weak point for clinical applications.

Kim *et al.* [15] have developed porous artificial bone scaffolds derived from hydroxyapatite (HA) by using PMMA as a porogen. They showed that the studied mechanical properties were affected by the porosity of the scaffolds. Still, the use of some organic additives, although necessary for manufacturing porous ceramics, degrades the quality of the final products. For this, these additives must be removed before the sintering step. Therefore, the final densification of the raw product is always preceded by a debinding step, its kinetics being of great importance and requiring a preliminary study. The added organic elements must be eliminated before the pores close to avoid the trapping of gases, a source of defects, which can damage the produced samples by inducing cracks.

However, the major disadvantages limiting the use of these porous compounds are their fragility and low mechanical resistance [16, 17], which are intimately linked to their microstructure, which depends on the synthesis and sintering conditions. [18, 19]. The association between hydroxyapatite HAP and tricalcium phosphate β-TCP develops a new biphasic biomaterial combining the characteristics of each mineral phase. Shiota *et al*. [20] densified two-phase 70HAP/30β-TCP powders by sintering at 1150°C after shaping under an isostatic pressure of 100 MPa, resulting in a density of approximately 98% and an average particle size of 0.8 μm. Es-saddik *et al*. [21] also studied the 60HAP/40β-TCP bioceramic, where the best densification (89%) and good diametral resistance (43MPa) were obtained at 1250°C. They concluded that the porosity of 11% and the presence of β-TCP or α-TCP phases being resorbable biomaterials is an advantage in accelerating the growth of bone tissue and contributing to bone adhesion at "implant-bone" interface without altering the mechanical characteristics. Despite the interesting properties of these biphasic materials, their use as an implant in the human body is limited to small implants with reduced mechanical load due to their weak mechanical characteristics. To solve the fragility constraints of ceramics derived from calcium phosphates, their association with inert oxides such as silica SiO_2 and zirconia ZrO_2 has been used to improve the mechanical properties of the composite formed and preserve the reactivity of calcium phosphate with living tissues [22, 23]. Unlike the SiO_2/HAP bioceramic linked to the solubility of silicon [24, 25], the ZrO_2/HAP composite with a microporous structure has mechanical properties close to biocortical bone [26]. Sina Khoshsima *et al*. [27] have studied the mechanical behavior of hydroxyapatite-zirconia-lanthanum oxide composites. As a result, adding ZrO_2 and La_2O_3 into the composites increased the diametral tensile strength. Alumina, Al_2O_3, is also a candidate widely involved in the mechanical reinforcement of ceramics and glass ceramics based on calcium phosphates. Thanks to its high stability and mechanical resistance, it was chosen as a good candidate for improving the mechanical characteristics of implanted biomaterials [8, 28]. Its combination with hydroxyapatite and tricalcium phosphate has been developed to cover good quality

resorption and mechanical strength sufficient to replace human bone. This work was devoted to the preparation of the HAP/β-TCP/Al_2O_3 biocomposite to improve the mechanical properties better. Applying the finite element method elucidates stationary cracks and shows the effects of crack interactions and the process of crack propagation under power.

2. Materials and Methods

In this study, we used commercial alumina (BDH chemicals, Ltd Poole England), commercial β-TCP (Fluka; Assay>96%), and synthesized hydroxyapatite (HAP) [29]. Powders of 60% wt HAP, 30% wt β-TCP, and 10% wt Al_2O_3 were mixed in 100 ml of bidistilled water and 50 ml of absolute ethanol, stirred for 20 h at room temperature and then dispersed in an ultrasonic bath for 20 min. The resulting mixture is filtered and dried in an oven at 80°C overnight. After calcining the powders at 800°C for 3 h, cylindrical specimens of 10 mm were compacted uniaxially under a load of 150 MPa. To better consolidate them, they were heat treated at different temperatures ranging from 1200°C to 1400°C for 3 h with a heating rate of 10°C min^{-1}.

The mechanical resistance of sintered specimens was measured by Brazilian tensile strength. The rupture strength (σr) was measured according to the following equation [21]: $\sigma_r = \frac{2F}{\pi.D.t}$ [Eq. 1], where F is the maximum applied load, D is the diameter, and t is the thickness of the disc. The tests are carried out using an LLOYD EZ50 device on cylindrical tablets of 8 mm in diameter and 2 mm thick measured out using a “0-150mm/0-6" digital caliper. The relative density of the ceramic is the ratio between the measured and theoretical densities. The Young's (E) and shear (G) moduli of the 60HAP/30β-TCP/10Al_2O_3 composite, as elastic moduli, were calculated by ultrasonic technique [30-31]. Young's E, and shear modulus G were derived from the longitudinal (V_L) and transversal (V_T) ultrasonic wave velocities. The testing apparatus consists of a short-duration pulse generator (Sofranel 5052 PR), which stimulated a broadband ultrasound emitter (Panametrics V 309) with a 5 MHz central frequency. By calculating the wave's propagation time delay in a specimen of thickness "e" ,the sound velocity was computed in accordance with the elastic theory, the V_L and V_T velocities are expressed with E and G modulus, density (ρ), and Poisson’s ratio (ϑ) :

$V_L = \sqrt{\frac{C}{\rho}} = \left(\frac{E(1-\vartheta)}{\rho(1+\vartheta)(1-2\vartheta)}\right)^{1/2}$ (Eq. 3); $V_T = \sqrt{\frac{G}{\rho}} = \left(\frac{E}{2\rho(1+\vartheta)}\right)^{1/2}$ (Eq. 4), where C is the longitudinal modulus.

The E and G modulus and the Poisson's ratio "υ" can be determined using the following formula: $G = \rho V_T^2$ (Eq. 5) ; $E = G\frac{3C-4G}{C-G}$ (Eq.6); $\vartheta = \frac{C-2G}{2(C-G)}$ (Eq. 7).

3. Results and Discussion

3.1. Chracterization.

After mixing the HAP, β-TCP, and Al_2O_3 powders, the HAP/β-TCP/Al_2O_3 composite was thermally treated progressively at 800°C then 1000°C. In this study, we are only interested in sintered ceramic at high temperatures between 1200-1400°C, whose XRD diagrams are shown in Fig.1. In addition to the primitive phases, other phases ($CaAl_2O_4$, $Ca_5Al_6O_{14}$, $Ca_2Al_2O_5$, and $Ca_3Al_2O_6$) appeared from 1200°C. Note that the intensity of the peaks related to HAP decreases when the sintering temperature increases. This is related to the

decomposition of HAP into β-TCP with their good reactivity with alumina, as well as the phase transformation of β-TCP into α-TCP above 1300°C [32, 33].

SEM images of bioceramic sintered at different temperatures are shown in Figure 2. An intergranular porosity was detected for the sintered ceramic at 1200°C (Fig.2a), while a dense structure was observed at 1300°C with the existence of some closed pores (Fig. 2b). At 1400°C, an increase in grain size was considered (Fig. 2c); this can affect the densification and the mechanical properties of this bioceramic.

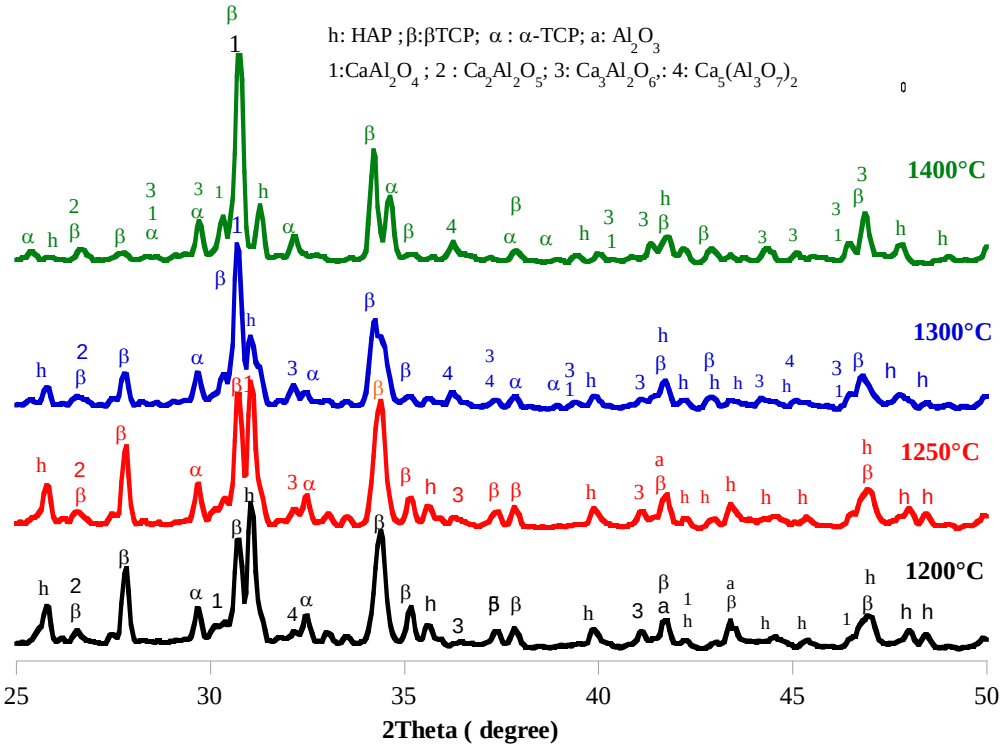

Figure 1. XRD patterns of 60HAP/30β-TCP/10Al_2O_3 sintered for 3h at **(a)** 1200, **(b)** 1250, **(c)** 1300, and **(d)** 1400°C.

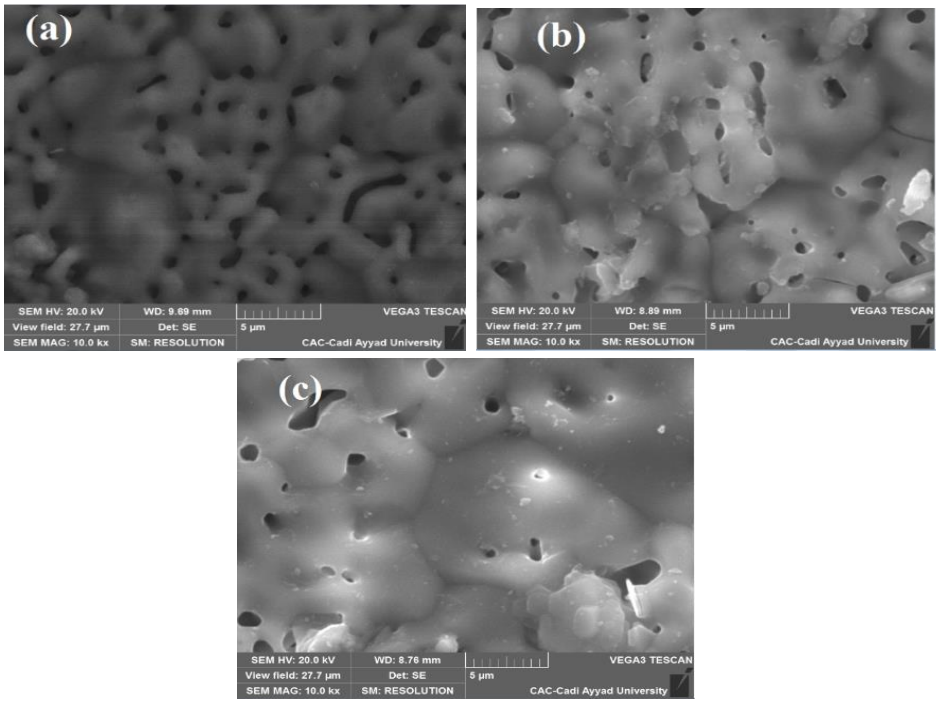

Figure 2. SEM images of ceramic sintered at various sintering temperatures: **(a)** 1250°C; **(b)** 1300°C; **(c)** 1400°C.

3.2. Densification and mechanical behavior.

The densification of the 60HAP/30β-TCP/10Al_2O_3 ceramic was modified with the sintering temperature (Fig. 3a). The best densification (71%) was obtained at 1250°C. This is related to the synergy between grain growth and the breakdown of HAP to β-TCP, which the last converts to α-TCP, forming several calcium aluminates phases of distinct theoretical densities. Note that a porosity of 29% is desirable to accelerate the growth of bone tissue despite its influence on the mechanical properties. At the same time, the presence of certain resorbable phases, such as β-TCP and α-TCP, contribute to the subsequent adhesion of the implant-bone interface and bone regrowth. Figure 3b shows the change of the diametral strength with the sintering temperature. The optimum rupture strength reached 23 MPa at 1250°C. Beyond this temperature, it decreases to 13 MPa at 1350°C, then improves slightly at 1400°C, which is related to the densification profile and the nature of the crystalline phases in the bioceramic.

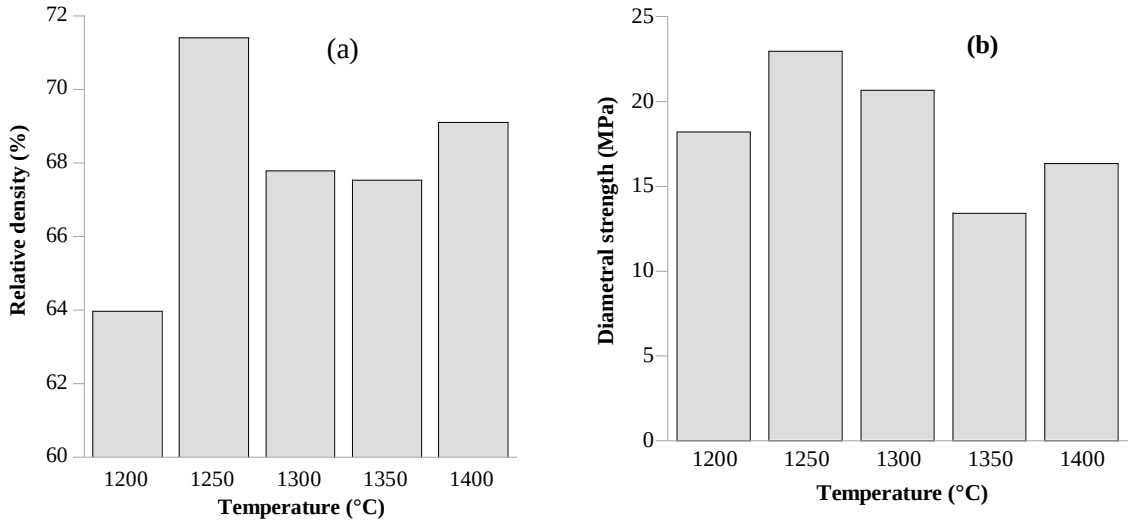

Figure 3. (a) Evolution of relative density of the bioceramic and **(b)** its evolution of diametral strength at various sintering temperatures.

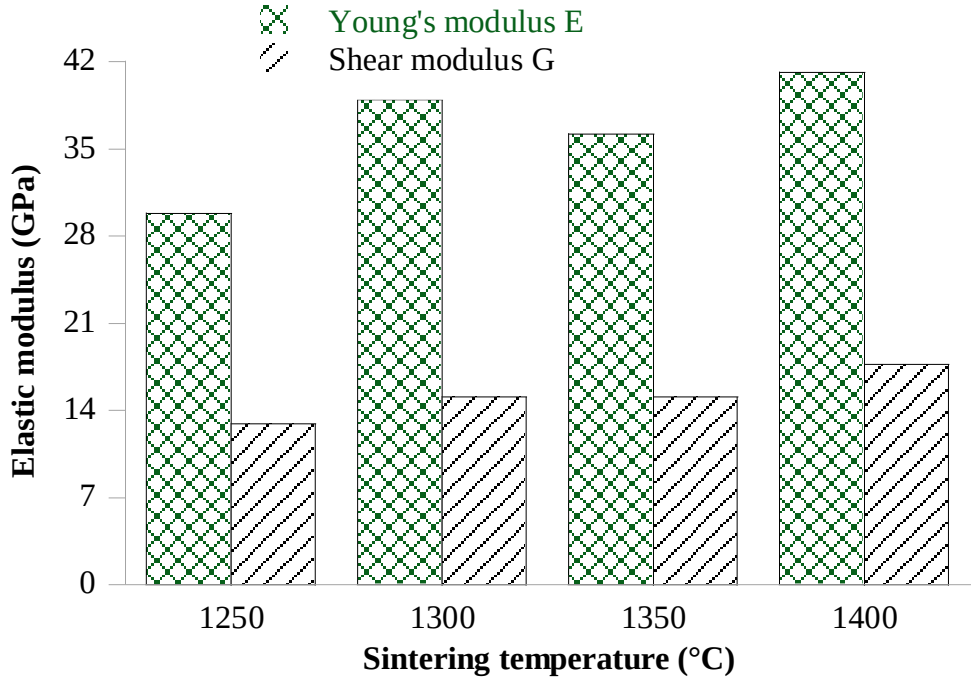

Figure 4. Young's and Shear's modulus of the ceramic as a function of sintering temperature.

The determination of the elasticity of the specimen with the sintering temperature is illustrated in Figure 4. Young's and shear moduli exceed 39 GPa and 15 GPa, respectively, at 1300°C, whereas they decrease at 1350°C and then increase intensively at 1400°C. This is in good relation with the size and the porosity of the grains as well as with the crystalline phases, which appeared after sintering.

From XRD and SEM data, the grain and pores sizes, r shape and distribution, as well as the formation of several phases such α-TCP and calcium aluminates after sintering can affect the densification and the mechanical properties of elaborate ceramics since the formed phases have different densities and coefficients of thermal expansion. These results agree with the observations made on the variations of the density and the mechanical properties of produced ceramics with the sintering process.

3.3 Numerical analysis of mechanical behavior of HAP/β-TCP/Al_2O_3 ceramics.

3.3.1. Finite element analysis.

The Finite Element Analysis (FEA) is an indispensable tool for improving design, assessing stress, locating critical zones, and predicting potential fracture origins CAST3M is a structural analysis calculation code through the finite element method [34]. The program is powerful, flexible, and optimized for the problems of elastic linear mechanics in static and dynamic, thermal problems, nonlinear problems (elastic materials, plastics, viscous), dynamics problems, etc. The language used to define the functional instructions of the process is a language named "GIBIANE" which allows, in particular, an easy exchange of information between the user and the program.

3.3.2. FEA boundary conditions.

Meshes are created by considering 4-node quadrilaterals in two dimensions (Fig.5). The experimental data are given in Table 1. Various loads of experimental forces F were applied to the arc defined by the angle 2ω of the sintered ceramic. The boundary conditions are taken so the arc EG is blocked in the y-axis.

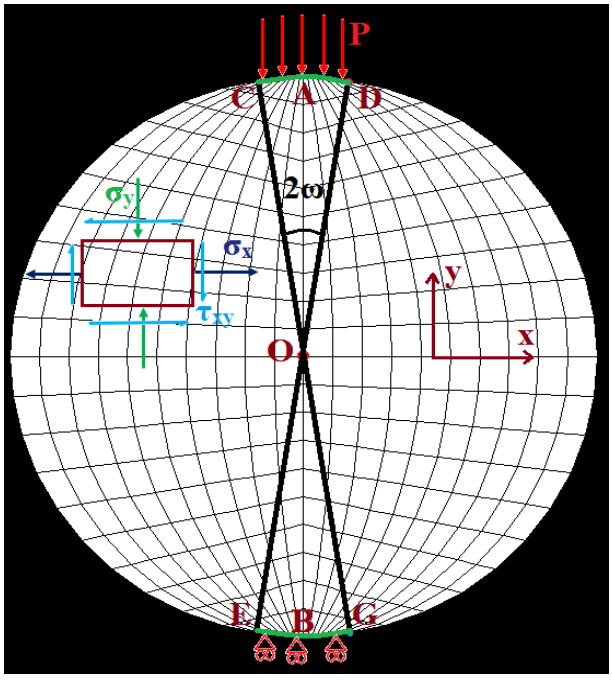

Figure 5. Meshes and boundary conditions.

Table 1. Characteristics of the studied bioceramic at various sintering temperatures.

Sintering Temperature (°C)	1250	1300	1350	1400
Thickness (mm)	2.09	2.23	2.33	2.37
Diameter (mm)	9.42	9.53	9.39	9.3
Young modulus (GPa)	29.86	38.96	36.19	41.13
Poisson ratio	0.1523	0.2889	0.2002	0.1614
Density (Kg/m^3)	2319	2180	2159	2218
Maximum force load (N)	710	690	461	566

The stresses applied to the loading plane, σ_{xx} and σ_{yy}, are then defined as follows [35]:

$$\sigma_{yy} = -\frac{2P}{\pi}\left[\frac{\left(1-\left(\frac{y}{R}\right)^2\right)sin2\omega}{1-2\left(\frac{y}{R}\right)^2 cos2\omega+\left(\frac{y}{R}\right)^4}+tan^{-1}\left(\frac{1+\left(\frac{y}{R}\right)^2}{1-\left(\frac{y}{R}\right)^2}tan\omega\right)\right] \quad (Eq.2)$$

$$\sigma_{xx} = \frac{2P}{\pi}\left[\frac{\left(1-\left(\frac{y}{R}\right)^2\right)sin2\omega}{1-2\left(\frac{y}{R}\right)^2 cos2\omega+\left(\frac{y}{R}\right)^4}-tan^{-1}\left(\frac{1+\left(\frac{y}{R}\right)^2}{1-\left(\frac{y}{R}\right)^2}tan\omega\right)\right] \quad (Eq.3)$$

Where 'R' is the radius of specimens, and 'P' is the applied pressure (MPa),

At the center of the disc, and when ω is small, $\sin2\omega \approx 2\omega$, and $F = P\omega Dt$, the principal stresses become: $\sigma_{yy}(0;0) = -\frac{6P\omega}{\pi} = -\frac{6F}{\pi Dt}$ $(Eq.4)$ and $\sigma_{xx}(0;0) = \frac{2P\omega}{\pi} = \frac{2F}{\pi Dt}$ $(Eq.5)$. The calculation of the equivalent stress $\sigma_G$was based on the sign of the tensile stress considered positive with $\sigma_{xx} \geq \sigma_{yy} \geq \sigma_{zz}$ according to the Griffith's theory [36, 21]: (i) when $3\sigma_{xx} + \sigma_{yy} \geq 0$; $\sigma_G = \sigma_{xx}$; (ii) when $3\sigma_{xx} + \sigma_{yy} < 0$; $\sigma_G = \frac{(\sigma_{xx}-\sigma_{yy})^2}{-8(\sigma_{xx}+\sigma_{yy})}$ $(Eq.6)$ and (iii) at the center of the disk $3\sigma_{xx} + \sigma_{yy} = 0$, $\sigma_G = \frac{2F}{\pi Dt}$ (Eq.7 equivalent to Eq.1).

3.3.3. Distribution of the stresses in the specimens.

Figure 6 shows the typical distribution of the principal stress fields σ_{xx} and σ_{yy} along the load diameter AB, in the samples sintered at 1250°C. For other calcination temperatures (1250, 1300, 1350 and 1400°C) the shape of their corresponding σ_{xx} and σ_{yy} curves are similar and the principal stress σ_{xx} remains constant along the diameter AB, which decreases in the vicinity of the contact band, becomes zero, and changes its sign (compression). If the 2ω angle is small, the traction cancels out very close to the periphery of the disc, which ensures greater distribution uniformity. However, the σ_{yy} stress increases from the center of the disc to the contact generator. The compression situation induces tensile stress perpendicular to the diameter of the loaded disk, which remains constant around the center, and rupture begins at the point of maximum tensile strength. The sample is broken along the diameter. On the other hand, we notice that the field of the principal stress σ_{xx} is intense around the center of the disc, and its value decreases as the angle 2ω increases, and the maximum values are recorded for the sintered ceramic at 1250°C. The variations of σ_{xx} and σ_{yy} along the loaded vertical diameter (AB) digitally simulated are in good agreement with the analytical solutions proposed elsewhere [21, 35]. It should be noted that an increase in the loading angle from 2ω = 5° to 2ω = 30° significantly reduces compressive stresses near the loaded boundaries on the disc. Hence, if the loading angle is increased, the probability of compression failure near the points of application of the force is reduced. As a result, cracks start from the center of the sample, and

this is a sign of the validity of the test. In addition, the same remarks must be made from the results found experimentally during the diametral compression test (Figure 7).

By comparing the mechanical resistance determined experimentally and that determined numerically by the finite element method, the Griffith criterion was used to calculate the sum $3\sigma_{xx} + \sigma_{yy}$, which is strictly less than zero at the center of the disc in our case. Using the equation 7, the diametral strength was determined by calculating the equivalent stress σ_G. The obtained theoretical results show that the maximum value of the equivalent stress is recorded almost at the center of the disc for the angles $2\omega \geq 20°$, which means that the crack is initiated around the center of the tablet. Figure 8 shows the similarity of the results found for the numerically calculated tensile stress and that measured experimentally, especially for $2\omega = 20°$. Therefore, the maximum breaking stress of the studied bioceramic is that obtained after sintering at 1250°C.

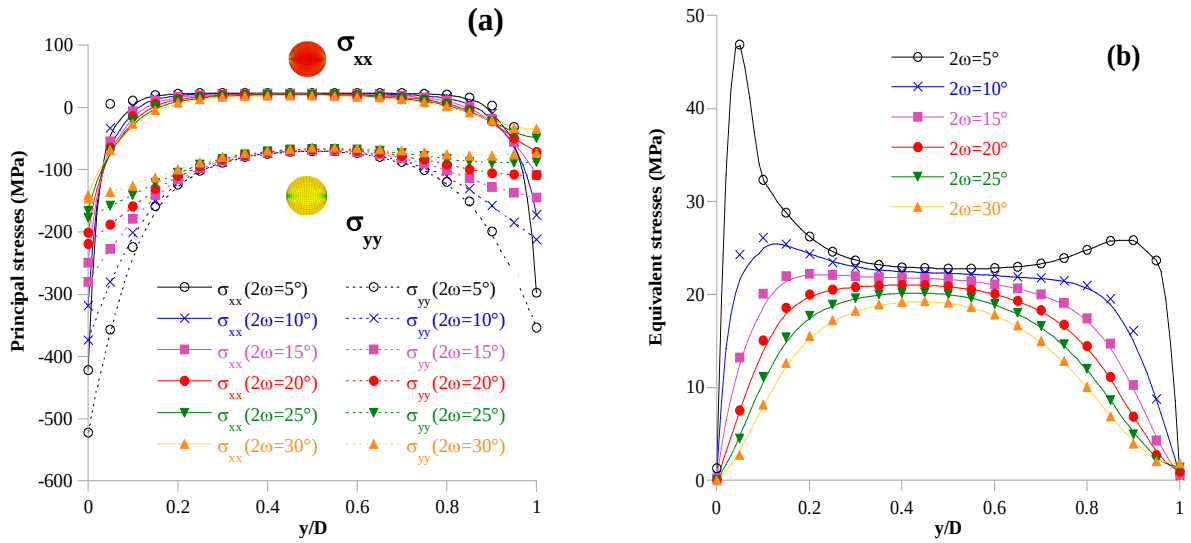

Figure 6. (a) Variation of $\sigma_{xx}$and σ_{yy} stress versus the normalized distance y/D, **(b)** The equivalent stress σ_G stress in the ceramic sintered at 1250°C, versus the normalized distance y/D in different contact angles 2ω.

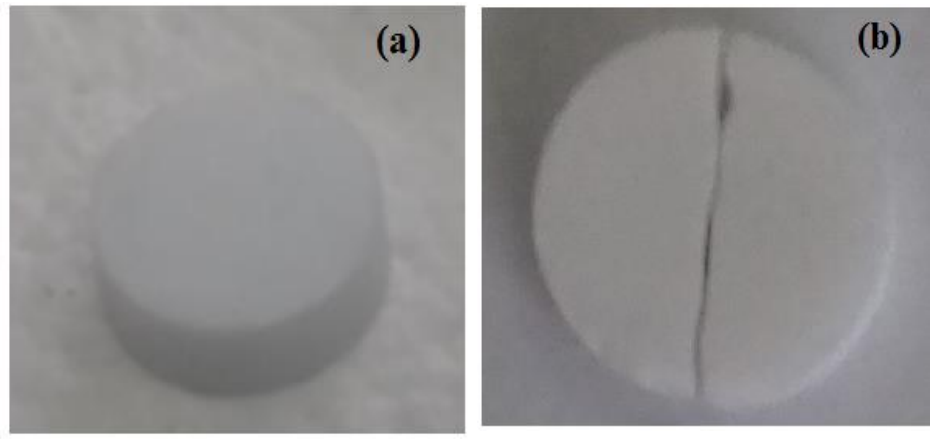

Figure 7. Photo of the disc before **(a)** and after diametral compression **(b).**

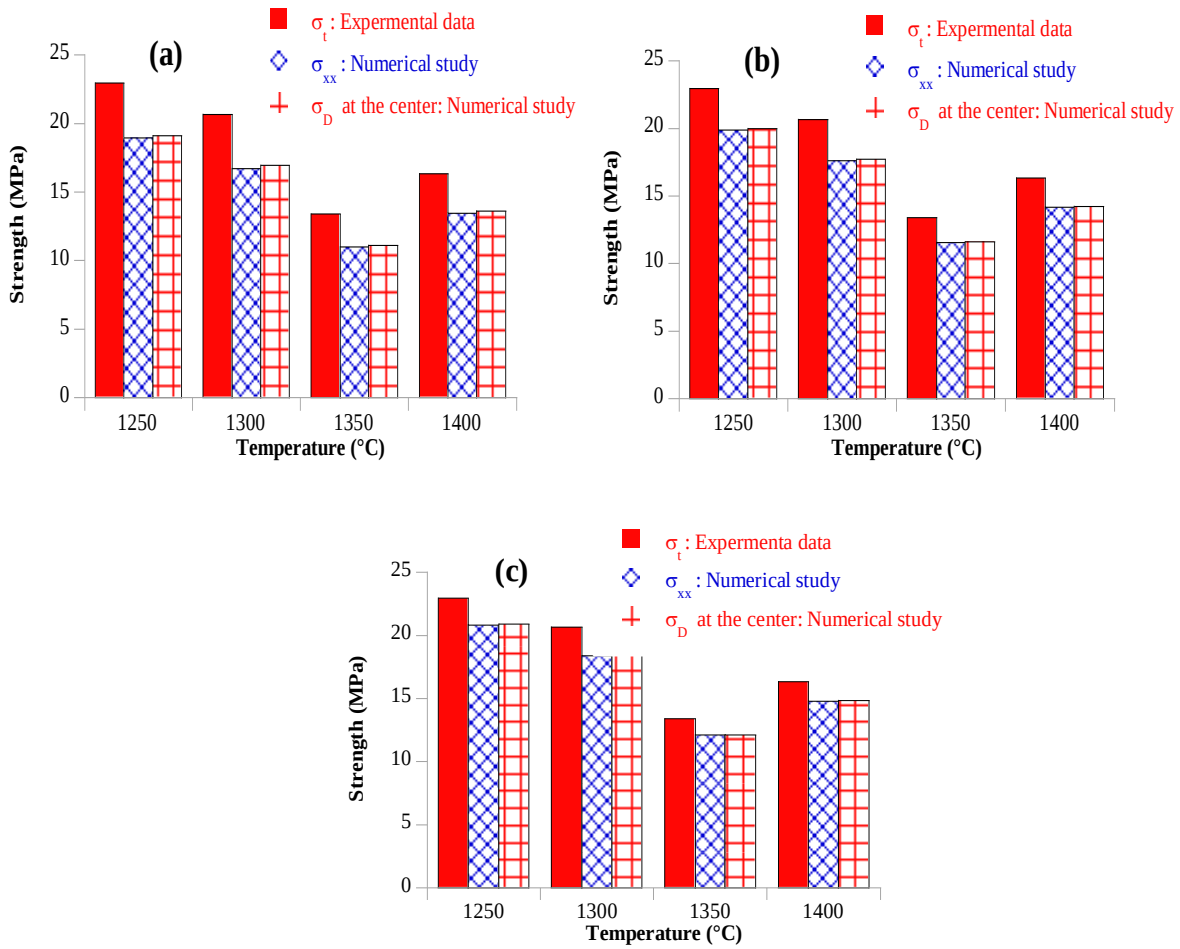

Figure 8. Comparative experimental and numerical data for **(a)** 2ω=30°, **(b)** 2ω=25° and **(c)** 2ω=20°.

The formation of new bone is in relation to the distribution of the stresses in repaired bone [37]. With suitable compressive stress acting on the bone tissue, the physiological fluid flows in the open junctions and some implant porosity. Shearing actions are created in the adjacent osteocytes and osteoblasts, which are beneficial for bone repair and growth [38]. The results presented in this work reveal that the compressive stress gradient distribution is stronger in the thinner thickness of the ceramic coatings. The simulated results revealed that the compressive stress gradient distribution is stronger in the thinnest section of the ceramic, which is more beneficial for bone regeneration because the thickness of this specimen is so thin that the effects of stress distribution in the bone. The maximum stresses are reduced when the ceramic is densified above 1250°C, reducing stress concentration. The predictive model can be used to investigate the micromechanical behavior of the studied bioceramic derived from the alumina-reinforced HAP/TCP composite, leading to significant elucidation of the failure processes of this biomaterial. These approaches can be extended to evoke damage mechanisms in materials and to control local strain fields around pores and their interactions. In fact, the specimen's topography, i.e., exaggerated porosity and fissures, largely affects the stress distribution. Several works have shown that the crack growth rate in a biomaterial is intensified when a crack initiates and propagates from a surface defect [39, 40].

Table 2. Mechanical properties of some published bioceramics and bone tissues.

Materials	$\sigma_t^{(a)}(MPa)$	$\sigma_c^{(b)}(MPa)$	$\sigma_f^{(c)}(MPa)$	$E^{(d)}(GPa)$	Ref.
HAP	4	-	45	108	[29;27]
β-TCP	5.3	-	50	97.5	[41, 42]

Materials	$\sigma_t^{(a)}(MPa)$	$\sigma_c^{(b)}(MPa)$	$\sigma_f^{(c)}(MPa)$	$E^{(d)}(GPa)$	Ref.
TCP–33.16 wt% FAp	7	95	15	80	[43]
β-TCP–40 wt% TiO_2	33	-	-	33,1	[44]
60HAP/40TCP	43	-	-	77,27	[21]
30HAP/70TCP	-	≈ 74	-	37,11	[45]
Cortical bone	50-130	88-180	50-150	12-22	[46-48]
Cancellous bone	-	2-12	10-20	0,084	[46,49-52]
Dentin	45-55	297	212	18	[49, 53-55]
Enamel	8-12	382	-	81-82	[49,56]
60HAP/30βTCP/10Al_2O_3	23	-	-	29-41	This study

[a]Tensile strength; [b]compressive strength, [c]Flexural strength, [d]Young's modulus

The comparison of the mechanical properties of elaborate ceramics with those described in the literature is very complex due to the wide variety of elaboration processes and mechanical tests. Generally, different mechanical tests other than the diametral method were used to characterize some bioceramics, such as three and four-point bending tests and compression tests. In addition, many parameters affect the mechanical characteristics of the produced samples, such as the morphology of initial powders, calcination treatment, grain size, sintering conditions, and the interfacial reaction of several composite constituents.

As our bioceramics are intended to be used as implant in the human body, it is necessary to compare them with bone tissue. Table 2 displays several values of the mechanical properties of bioceramics and representative bone tissues described in the literature. The optimal Young's modulus obtained for the 60HAP/30β-TCP/10Al_2O_3 ceramic (41 GPa) is higher than that of dentin and cortical bone but lower than that of the enamel and close to β-TCP-40 wt% TiO_2 developed by Ayadi *et al*. [44].

The rupture strength depends on the mechanical test method, and the obtained optimum value in this work (23 MPa) is superior to that of enamel and to those of pure HAP, pure β-TCP, and TCP–33.16 wt% FAp composite, which has a tensile strength of 4 MPa, 5,3 MPa, and 7 MPa, respectively [27, 42, 43], and lower than that of dentin. Consequently, the mechanical characteristics obtained are acceptable for a bone graft with a porosity around 30%, which is desirable to accelerate the growth of the bone tissue.

4. Conclusion

This study was mentioned in a global approach from synthesizing powders to the characterization of sintered 60HAP/30β-TCP/10Al_2O_3 bioceramic for orthopedic applications. Experimentally, we varied the sintering temperature to follow the evolution of the structure, the microstructure, and the mechanical behavior of the bioceramics. According to the sintering temperature, their rupture strength was measured by the Brazilian test, and it reached a maximum value of 23 MPa at 1250°C, an acceptable value for a bone graft. Thus, the results obtained are very promising and demonstrate the improvement of the mechanical properties of the composite compared to the pure individual phases. Observation of the microstructure suggests thermal action on the bioceramic topography with slight grain growth and persistence of minor porosity, and there is good particle-matrix interface bonding. The main stress distribution in the ceramic determined by the finite element method is well correlated with the experimental results. Consequently, alumina reinforced with HAP/β-TCP composite is mechanically compatible with bone grafting and may be a potential material for bone repair.

Funding

This research received no external funding.

Acknowledgments

Thanks to everyone who helped with this work

Conflicts of Interest

The authors declare no conflict of interest.

References

1. Varadavenkatesan, T.; Vinayagam, R.; Pai,P.; Brindhadevi, K.; Pugazhendhi, A.; Selvaraj, R. Synthesis, biological and environmental applications of hydroxyapatite and its composites with organic and inorganic coatings. *Prog. Org. Coat.* **2021**, *151*, 106056, https://doi.org/10.1016/j.porgcoat.2020.106056
2. Kim, Y.; Bae,J.; Uyama, E.; Sekine, K.; Kawano, F.; Hamada, K. Effects of zirconia additives on β-tricalcium-phosphate cement for high strength and high injectability. *Ceram. Int.* **2021**, *47*, 1882-1890, https://doi.org/10.1016/j.ceramint.2020.09.017
3. Wang, J.; Wang, D.G.; Li, X.T.; Zhai, J.Q.; Lu, G.X. ; Chen, C.Z. Characteristics of β-tricalcium phosphate/ZrO_2 composite films deposited by pulsed laser deposition at different laser fluences. *Ceram. Int.* **2022**, *48*, 34437-34445, https://doi.org/10.1016/j.ceramint.2022.08.023
4. Duarte Macedo, F.; Ana Cunha, F.; Mano, F.J.; Oliveira, B.M.; Silva, P.A. Tricalcium phosphate doped with Mg^{2+} and combinations of Mn^{2+}, Zn^{2+} and Fe^{3+}: A DoE study on sintering, mechanical, microstructural and biological properties. *Ceram. Int.* **2022**, *48*, 20467-20477, https://doi.org/10.1016/j.ceramint.2022.04.004
5. Sokolova, V. ; Matthias Epple, M. Biological and Medical Applications of Calcium Phosphate Nanoparticles. *Chem. Eur. J.*, **2021**, *27*, 7471 – 7488, https://doi.org/10.1002/chem.202005257
6. Abdul Halim, N.A.; Hussein, MZ.; Kandar, MK. Nanomaterials-Upconverted Hydroxyapatite for Bone Tissue Engineering and a Platform for Drug Delivery. *Int. J. Nanomed.* **2021,** *16*, 6477-6496, https://doi.org/10.2147/IJN.S298936
7. Azevedo-Silva, L.J.; Padovini, D.S.S.; Ferrairo, B.M.; Minim, P.R.; Pereira, L.F. ; Monteiro, R.S.; Fortulan, C.A.; Lisboa-Filho, P.N.; Borges, A.F.S. Ceramic Composites from Bovine Hydroxyapatite, ZrO_2@SiO_2, and Hydroxyapatite+15%ZrO_2@SiO_2. *Dent. Mater.* **2022**, *38*, e39-e40, https://doi.org/10.1016/j.dental.2021.12.094
8. Yu, W.; Wang, X.; Zhao, J.; Tang, Q.; Wang, M.; Ning, X. Preparation and mechanical properties of reinforced hydroxyapatite bone cement with nano-ZrO_2. *Ceram. Int.* **2015**, *41*, 10600-10606. https://doi.org/10.1016/j.ceramint.2015.04.159.
9. Alturki, A.M.; Abu-Rayyan, A.; Abualnaja, K.M.; Alhashmialameer, D.; El-Saeed, R.A.; El-Shabasy, R.M. Physicomechanical and morphological properties of hydroxyapatite nanocrystals substituted with copper–zirconium. *J Mater Sci Technol*. **2021**, *14*, 2312-2321, https://doi.org/10.1016/j.jmrt.2021.06.097
10. Soon, Y.M.; Shin, K.-H.; Koh, Y.H.; Lee, J.H.; Choi, W.Y.; Kim, H.E. Fabrication and compressive strength of porous hydroxyapatite scaffolds with a functionally graded core/shell structure. *J. Eur. Ceram. Soc.* 2011, *31*, 13–18, https://doi.org/10.1016/j.jeurceramsoc.2010.09.008.
11. Hammel, E.; Ighodaro, O.-R.; Okoli, O. Processing and properties of advanced porous ceramics: An application based review. Ceram. Int. 2014, 40, 15351–15370, https://doi.org/10.1016/j.ceramint.2014.06.095.
12. Geetha, B.; Premkumar, J.; Paul Pradeep, J.; Krishnakumar, S. Synthesis and characterization of bioscaffolds using freeze drying technique for bone regeneration. *Biocatal. Agric. Biotechnol*. **2019**, *20*, 101184. https://doi.org/10.1016/j.bcab.2019.101184
13. Jun, Y.K.; Kim, W. H.; Kweon, O.K.; Hong, S.-H. The fabrication and biochemical evaluation of alumina reinforced calcium phosphate porous implants. *Biomaterials*, **2003**, *24*, 3731-3739, https://doi.org/10.1016/S0142-9612(03)00248-5

14. Gain, A.K.; Zhang, L.; Liu, W.; Microstructure and material properties of porous hydroxyapatite -zirconia nanocomposites using polymethyl methacrylate powders. *Mater. Des.* **2015**, *67*, 136–144 http://dx.doi.org/10.1016/j.matdes.2014.11.028
15. Kim , T.R.; Kim , M.S; Goh, T.S.; Lee, J.S.; Kim , Y. H.; Yoon, S.-Y.; Lee, C.-S., Evaluation of Structural and Mechanical Properties of Porous Artificial Bone Scaffolds Fabricated via Advanced TBA-Based Freeze-Gel Casting Technique. *Appl. Sci.* **2019**, *9*, 1965, https://doi.org/10.3390/app9091965
16. Ielo, I.; Calabrese, G.; De Luca,G.; Conoci, S. Recent Advances in Hydroxyapatite-Based Biocomposites for Bone Tissue Regeneration in Orthopedics. *Int. J. Mol. Sci*. **2022**, *23*, 9721, https://doi.org/10.3390/ijms23179721
17. Fiume, E.; Magnaterra, G.; Rahdar , A.; Verné, E.; Baino, F. Hydroxyapatite for Biomedical Applications: A Short Overview. *Ceramics* ***2021***, *4*, 542–563, https://doi.org/10.3390/ceramics4040039
18. Descamps, M., Richart, O., Hardouin, P., Hornez, J. C., Leriche, A. Synthesis of macroporous β-tricalcium phosphate with controlled porous architectural. *Ceram. Int.* **2008**, *34*, 1131-1137. https://doi.org/10.1016/j.ceramint.2007.01.004
19. Chen, B.H.; Chen, K.I.; Ho, M.L.; CHen, H.N.; Chen, W.C.; Wang, C.K. Synthesis of calcium phosphates and porous hydroxyapatite beads prepared by emulsion method. *Mater.Chem. Phys*. **2009**, *113*, 365-371, https://doi.org/10.1016/j.matchemphys.2008.06.040
20. Shiota, T.; Shibata, M.; Yasuda, K.; Matsuo, Y. Influence of β-tricalcium phosphate dispersion on mechanical properties of hydroxyapatite ceramics. *J. Ceram. Soc. Jp.* **2008**, *116*, 1002-1005. https://doi.org/10.2109/jcersj2.116.1002
21. Es-Saddik, M.; Laasri, S.; Laghzizil, A.; Nunzi, J.M.; Taha, M.; Guidara, A.; Hajjaji, A.; Bouaziz, J. Mechanical strength characterization and modeling of hydroxyapatite/tricalcium phosphate biocomposite using the diametral-compression test. *Eur. Phys. J. Appl. Phys*. **2021**, *93*, 30403, https://doi.org/10.1051/epjap/2021200368
22. Rao, R.R.; Kannan, T.S. Synthesis and sintering of hydroxyapatite–zirconia composites, Mater. Sci. Eng. C **2002**, *20*, 187-193, https://doi.org/10.1016/S0928-4931(02)00031-0
23. Mobasherpour, I.; Solati Hashjin, M. ; Razavi Toosi, S.S. ; Darvishi Kamachali, R. Effect of the addition ZrO_2-Al_2O_3 on nanocrystalline hydroxyapatite bending strength and fracture toughness. *Ceram. Int.* **2009**, *35*, 1569-1574, https://doi.org/10.1016/j.ceramint.2008.08.017
24. Xu, J.L.; Khor, K.A. Chemical analysis of silica doped hydroxyapatite biomaterials consolidated by a spark plasma sintering method, *J.Inorg.Biochem.* **2007**, *101*, 187-195, https://doi.org/10.1016/j.jinorgbio.2006.09.030
25. Borum, L.; Wilson, O. C. Surface modification of hydroxyapatite. Part II. Silica, *Biomaterials* **2003**, *24*, 3681-3688**,** https://doi.org/10.1016/s0142-9612(03)00240-0
26. Htun, Z. L. ; Ahmad, N. ; Thant, A.A.; Noor, A.F.M. Characterization of CaO-ZrO_2 reinforced HAP biocomposite for strength and toughness improvement. *Procedia Chem.* **2016**, *19*, 510-516, https://doi.org/10.1016/j.proche.2016.03.046
27. Khoshsima, S., B.Yilmaz , Tezcaner , A.; Z. Evis, Structural, mechanical and biological properties of hydroxyapatitezirconia-lanthanum oxide composites. *Ceramics International* **2016**, *42*,15773–15779, http://dx.doi.org/10.1016/j.ceramint.2016.07.041
28. Barkallah, R. ; Taktak, R. ; Guermazi, N. ; Elleuch, K. ; bouaziz, J. Mechanical properties and wear behaviour of alumina/tricalcium phosphate/titania ceramics as coating for orthopedic implant. *Engineering Fracture Mechanics* **2021**, *241*, 107399, https://doi.org/10.1016/j.engfracmech.2020.107399
29. Laasri, S. ; Taha, M. ; Laghzizil, A. ; Hlil, E.K. ; Chevalier. The affect of densificatio n and dehydroxylation on the mechanical prop erties of stoichiometric hydroxyapatite bioceramics, *J.Mater. Res. Bull***.** **2010**, *45*, 1433–1437, https://doi.org/10.1016/j.materresbull.2010.06.040
30. Banouni, H. ; Khatib, K. ; Ouacha, E. ; Faiz, B. ; Aboudaoud, I. ; Mesbah, H. Ultrasound Non-Destructive Characterization of Early Hydration of Cement Pastes: The Effects of Water-Cement Ratio and Curing Temperature, Annales de Chimie - *Science des Matériaux* **2022**, *46*, 307-312, https://doi.org/10.18280/acsm.460604
31. Es-saddik, M. ; Laasri, S. ; Taha, M. ; Laghzizil, A ; Guidara, A . ; Chaari,K. ; Bouaziz, J. ; Hajjaji, A. ; Nunzi J.M. Effect of the surface chemistry on the stability and mechanical properties of the Zirconia-Hydroxyapatite bioceramic. *Surface. Interf.* **2021**, *23*, 100980, https://doi.org/10.1016/j.surfin.sa2021.100980.

32. Gutiérrez-Alejandre, A. ; Gonzalez-Crus, M. ; Trombetta, M. ; Busca, G. ; Ramirez, J. Characterization of alumina–titania mixed oxide supports: Part II: Al_2O_3-based supports. *Microp. Mesop. Mat.* **1998**, *23*, 265-275, https://doi.org/10.1016/S1387-1811(98)00121-8
33. *Tayebia, S. ; Mirjalilib, F. ; Samadi, H. ; -Nemati, A.* The effect of additives on the properties of HAp-Al_2O_3 nano-composite powders. *J. Ceram. Proces. Res.* **2016**, *17*,1033-1041, https://doi.org/10.36410/jcpr.2016.17.10.1033
34. Accueil | Cast3M (cea.fr);
35. Hondros, G. The evaluation of Poisson's ratio and the modulus of materials of low tensile resistance by the Brazilian (indirect tensile) test with particular reference to concrete. *Aust. J. Appl. Sci.* **1959**, *10*, 243-268, https://cir.nii.ac.jp/crid/1570572700502715136.
36. Nicola M. Pugno, The centenary of Griffith's theory. *Matter* **2021**, *4*, 3811-3813, https://doi.org/10.1016/j.matt.2021.11.002
37. Tuner, C.H. ; Forwood, M.R. ; Otter, M.W. Mechanotransduction in bone: Do bone cells act as sensors of fluid flow?, *FASEB Journal*, **1994**, *8*,875- 878, https://doi.org/10.1096/fasebj.8.11.8070637
38. Reich, K.M. ; Gay, C.V. ; Frangos, J.A. Fluid shear stress as a mediator of osteoblast cyclic adenosine monophosphate production. *J. Cell. Physiol.* **1990**, *143*, 100-104, https://doi.org/10.1002/jcp.1041430113
39. Dezecot, S. ; Maurel, V. ; Buffiere, J.-Y. ; Szmytka, F. ; Koster, A. 3D characterization and modeling of low cycle fatigue damage mechanisms at high temperature in a cast aluminum alloy. *Acta Mater.* **2017**, *123*, 24-34, https://doi.org/10.1016/j.actamat.2016.10.028
40. Serrano-Munoz, I. ; Buffiere, J.Y. ; Verdu, C. ; Gaillard, Y. ; Mu, P. ; Nadot, Y. Influence of surface and internal casting defects on the fatigue behaviour of A357-T6 cast aluminium alloy. *Int. J. Fatigue* **2016**, *82*,361-370, https://doi.org/10.1016/j.ijfatigue.2015.07.032
41. Laasri, S. ; Taha, M. ; Hlil, E.K. ; Laghzizil, A. ; Hlil, E.K. ; Hajjaji, A. Manufacturing and mechanical properties of calcium phosphate biomaterials. *C. R. Mecanique* **2012**, *340*, 715–720, http://dx.doi.org/10.1016/j.crme.2012.09.005
42. Bouslama, N.; Ben Ayed, F. ; Bouaziz, J. Sintering and mechanical properties of tricalcium phosphate-florapatite composites. *Ceram. Int.* **2009**,*35*,1909–1917, https://doi.org/10.1016/j.ceramint.2008.10.030
43. Elghazel, A. ; . Taktak, R. ; Bouaziz, J. Combined numerical and experimental mechanical characterization of a calcium phosphate ceramic using modifi ed Brazilian disc and SCB specimen. *Materials Science & Engineering A* **2016**, *670*, 240–251, http://dx.doi.org/10.1016/j.msea.2016.06.020
44. Ayadi,I.; Ben Ayed, F. ; Sintering and the mechanical properties of the tricalcium phosphate/titania composites. *J. Mech. Behav. Biomed.* **2015**, *49*, 129–140. http://dx.doi.org/10.1016/j.jmbbm.2015.05.001
45. Mehmet Y etmez, Sintering Behavior and Mechanical Properties of Biphasic Calcium Phosphate Ceramics. *Advances in Advances in Materials Science and Engineering*, **2014**, 1-5 – 2014, https://doi.org/10.1155/2014/871749
46. J.C. Elliott. Structure and Chemistry of the Apatite and Other Calcium Orthophosphates, Elsevier Science BV, Amsterdam, **1994**, eBook ISBN: 9781483290317 https://www.elsevier.com/books/structure-and-chemistry-of-the-apatites-and-other-calcium-orthophosphates/elliott/978-0-444-81582-8.
47. Turner, C.H. ; Chandran, A. ; Pidaparti, R.M.V. The anisotropy of osteonal bone and its ultrastructural implications. *Bone* **1995**, *17*, 85–89. https://doi.org/10.1016/8756-3282(95)00148-7
48. Jae-Young Rho , Liisa Kuhn-Spearing , Peter Zioupos. Mechanical properties and the hierarchical structure of bone. *Medical Engineering & Physics* **1998**, *20*, 92-102, https://doi.org/10.1016/S1350-4533(98)00007-1.
49. Hench, L.L. , An Introduction to Bioceramics, Chapter 37: Characterization of Bioceramics, World Scientific Publishing Co. Pte. Ltd., Singapore 1993, pp. 521–540, ISBN 978-1-908977-15-1 .
50. Ravaglioli, A. ; Krajewski, A. Bioceramics: Materials, Properties and Applications, Published By Chapman & Hall, London, England **1992**, p. 422, https://link.springer.com/book/10.1007/978-94-011-2336-5.
51. Shi, D. Biomaterials and Tissue Engineering, Springer, Berlin Heidelberg, New York 2004, pp. 2–200, https://link.springer.com/book/10.1007/978-3-662-06104-6.
52. Carter, D.R. ; Hayes, W.C. The compressive behaviour of bone as a two-phase porous structure. *J. Bone Jt. Surg*. **1977**, *59*, 954–962, https://pubmed.ncbi.nlm.nih.gov/561786/.
53. Chun, K.J. ; Choi, H.H. ; Lee, J.Y. Comparison of mechanical property and role between enamel and dentin in the human teeth, J. Dent. Biomech. 2014,5 1–6. https://doi.org/10.1177/1758736014520809

54. Craig, R.G. ; Peyton, F. Elastic and mechanical properties of human dentin. *J. Dent. Res*. **1958**, *37*, 710–718. https://doi.org/10.1177/00220345580370041801
55. Plotino, G. ; Grande, N.M. ; Bedini, R. ; Pameijer, C.H. ; Somma, F. Flexural properties of endodontic posts and human root dentin. *Dental materials* **2007**, 2 3, 1129–1135, https://doi.org/10.1016/j.dental.2006.06.047
56. El-Mowafy, O.M. ; Watts, D.C. Fracture toughness of human dentin. *J. Dent. Res.* **1986**, *65*, 677–681 . https://doi.org/10.1177/00220345860650050901